Particle Accelerators, 1987, Vol. 21, pp. 1–27
Photocopying permitted by license only

Printed in the United States of America

BEAM TRAPPING IN A MODIFIED BETATRON WITH TORSATRON WINDINGS†

C. A. KAPETANAKOS
Advanced Beam Technologies Branch, Plasma Physics Division, Naval Research Laboratory, Washington, DC 20375

D. DIALETIS
Science Applications International Corporation, McLean, VA 22102

and

S. J. MARSH
Sachs/Freeman Associates, Bowie, MD 20715

(Received July 5, 1985; in final form June 10, 1986)

The guiding-center equations for the reference electron located at the centroid of an intense electron ring confined in a torsatron-assisted modified betatron field are derived by time averaging its fast motion. These "slow" equations are integrated analytically to obtain the nonlinear orbits for the guiding center. In addition, from the guiding-center equations, we have obtained a nonlinear expression that predicts very accurately the ring equilibrium position, even for large displacements from the minor axis of the torus. These results have provided an invaluable insight into the development of a trapping scheme. The proposed scheme is compatible with the slow acceleration of the modified betatron and is based on a low-amplitude, rapidly varying magnetic field that shifts the ring equilibrium position from near the wall to the minor axis of the torus in a time shorter than a beam bounce period.

1. INTRODUCTION

Extensive theoretical studies[1–20] over the last few years have shown that the modified betatron accelerator has the potential to generate electron beams of very high current. Recently, a "table top" device[21] at the University of California, Irvine, has produced electron rings with about 200 A of circulating current. A larger device, currently under test at the Naval Research Laboratory,[22] has been designed to produce multi-kiloampere electron rings and to address the critical physics issues of the modified betatron concept.

A disadvantage of the modified betatron accelerator is its sensitivity to energy mismatch.[2] Whenever the energy of the electron beam is not precisely matched to the betatron magnetic field, the center of beam gyration in the plane transverse to the minor axis is shifted radially, and thus the probability for the beam to strike the wall increases. To alleviate the energy mismatch problems, a modified

† This work was supported by the Strategic Defense Initiative Organization and by the Office of Naval Research.

betatron accelerator should be carefully designed to provide an accurate and precise betatron field, and the injector accelerator should generate electron pulses having an energy that precisely matches this field.[22]

To reduce the orbit sensitivity of the modified betatron to the energy mismatch, Roberson *et al.* have suggested[23] the use of a strong focusing field generated by $l = 2$ stellarator windings. In more recent studies,[24] we have demonstrated numerically that the energy bandwidth of a modified betatron configuration assisted by a strong focusing field generated by torsatron windings can be very wide. In addition, we have shown that the torsatron windings also substantially improve the current-carrying capabilities of the device[24] and could alleviate the beam displacement problem associated with the diffusion of the self-magnetic-field.

However, the usefulness of the twisted windings in improving the performance of the modified betatron remained questionable, because a scheme to trap the beam in such a configuration was not available. By reducing the orbit sensitivity to the energy mismatch, the strong focusing field makes trapping of the beam in such devices more difficult.

Recently Sprangle and Kapetanakos[25] have developed a scheme for trapping a beam in a rebatron accelerator. This device has a magnetic field configuration that is similar to that of a modified betatron supplemented with torsatron windings. The suggested scheme is based on the dissipative force generated by the resistive wall surrounding the electron ring. Although such a trapping scheme is appropriate for a rebatron, it is of doubtful usefulness for the modified betatron. The reason is that in the rebatron the particle acceleration occurs very rapidly, i.e., over a few microseconds, and therefore the cyclotron frequency corresponding to the betatron magnetic field (Ω_{z0}/γ) varies rapidly with time. Therefore, the resistive wall mode may not impose serious limitations on the stability of the ring. However, this is not the case in the modified betatron, because the acceleration occurs slowly, i.e., over a few milliseconds.

In this paper we propose a trapping scheme that is compatible with the slow acceleration of the modified betatron. The proposed trapping approach is based on a low-amplitude, rapidly varying magnetic field that shifts the beam equilibrium position near the minor axis of the torus in a time shorter than the beam bounce period. Since the new trapping scheme is similar to that presently used in the NRL modified betatron,[13,14] its implementation would require only minor modifications in the existing device.

Before addressing the beam trapping, we derive two equations that describe the nonlinear motion of the guiding center of the reference electron that is located at the beam centroid. Using these equations, we obtain a nonlinear expression that accurately predicts the beam equilibrium position, even for large displacement from the minor axis of the torus. In addition, by integrating analytically the guiding-center equations, we obtain an approximate constant of the motion that predicts the topology of the guiding-center orbits. These analytical results have provided an invaluable insight into the development and understanding of the trapping scheme.

2. GUIDING-CENTER MOTION

In this section, we derive the equations describing the guiding-center motion for the reference electron that is located at the centroid of an electron beam with a circular cross section. In the system of coordinates shown in Fig. 1, the instantaneous position of the reference electron is

$$r = r_0 + X + \delta r, \tag{1}$$

$$z = Z + \delta z, \tag{2}$$

where r_0 is the major radius of the torus, X and Z define the position of the guiding center relative to the minor axis, and δr and δz give the position of the gyrating electron relative to the guiding center.

Introducing the complex variables

$$u = r + iz, \tag{3}$$

$$U = X + iZ, \tag{4}$$

$$\delta u = \delta r + i\delta z, \tag{5}$$

and combining Eqs. (1) through (5), we obtain

$$u = r_0 + U + \delta u. \tag{6}$$

Substituting Eq. (3) and its time derivative into the equations of motion

$$\frac{d}{dt}(\gamma \dot{r}) - \gamma r \dot{\theta}^2 = -\frac{e}{m}\left[E_r + \frac{1}{c}(r\dot{\theta}B_z - \dot{z}B_\theta)\right]$$

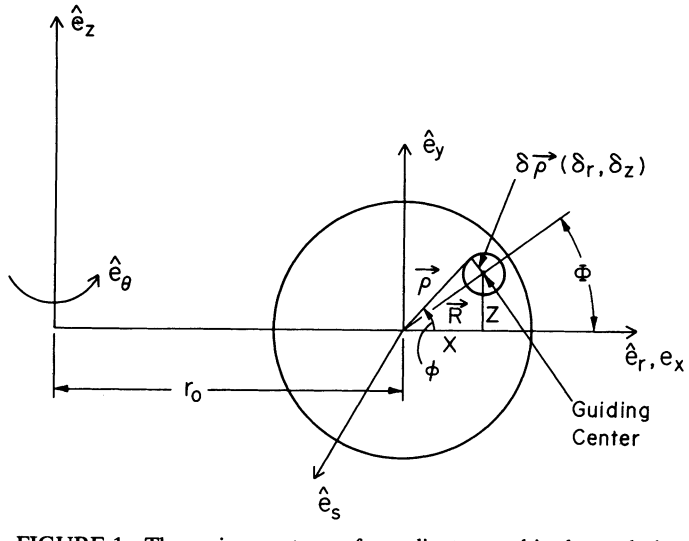

FIGURE 1 The various systems of coordinates used in the analysis.

and

$$\frac{d}{dt}(\gamma\dot{z}) = -\frac{e}{m}\left[E_z + \frac{1}{c}(\dot{r}B_\theta - r\dot{\theta}B_r)\right],$$

we obtain

$$\ddot{U} + \left(\frac{\dot{\gamma}}{\gamma} + i\frac{\Omega_\theta}{\gamma}\right)\dot{u} - \frac{v_\theta^2}{r} = -\frac{e}{m\gamma}\left[(E_r + iE_z) - \frac{iv_\theta}{c}(B_r + iB_z)\right], \tag{7}$$

where Ω_θ is the cyclotron frequency corresponding to the toroidal magnetic field B_θ, v_θ is the toroidal velocity, E_r and E_z are the image electric fields, and B_r and B_z are the components of applied (torsatron and betatron) and image magnetic fields.

2.1. *Applied Magnetic Fields*

The toroidal magnetic field consists of the applied toroidal field and that generated by the torsatron windings. To lowest order the toroidal field is given by[24]

$$B_\theta = -(B_0 + B_s^{ex}) + B_s^{ex}\varepsilon_t I_2(2\alpha\rho)(e^{2i(\phi-\alpha s)} + e^{-2i(\phi-\alpha s)}), \tag{8}$$

where B_0 and B_s^{ex} are defined in the local coordinate system $\hat{e}_x$, $\hat{e}_y$, $\hat{e}_s$; $B_0 = 8\pi I/cL$ (here I is the current and L is the period of the torsatron windings); $B_s^{ex}\varepsilon_t = 2\alpha B_0\rho_0 K_2'(2\alpha\rho_0)$, in which ρ_0 is the minor radius of the torsatron windings; K_2 and I_2 are the modified Bessel functions; and $\alpha = 2\pi/L$.

Since, for relativistic energies, v_θ is approximately constant,

$$\omega_w = 2\alpha v_\theta \approx -2\alpha s/t, \tag{9}$$

and Eq. (8) becomes

$$B_\theta = -(B_0 + B_s^{ex}) + B_s^{ex}\varepsilon_t I_2(2\alpha\rho)(e^{2i\phi}e^{i\omega_w t} + e^{-2i\phi}e^{-i\omega_w t}). \tag{10}$$

Similarly, to the lowest order, the components of the torsatron field transverse to the minor axis are[24]

$$B_\rho^t = 2B_s^{ex}\varepsilon_t I_2(2\alpha\rho)\sin[2(\phi - \alpha s)], \tag{11}$$

$$B_\phi^t = \frac{2B_s^{ex}\varepsilon_t}{\alpha\rho} I_2(2\alpha\rho)\cos[2(\phi - \alpha s)]. \tag{12}$$

These expressions are for a cylindrical system, and thus the toroidal corrections have been omitted. Therefore, the analytical work assumes implicitly that the net vertical field of the unidirectional torsatron windings is cancelled by outboard coils.

Substituting Eqs. (11) and (12) into the expressions for B_r^t and B_z^t,

$$B_r^t = B_\rho^t\cos\phi - B_\phi^t\sin\phi, \tag{13}$$

$$B_z^t = B_\rho^t\sin\phi + B_\phi^t\cos\phi, \tag{14}$$

and using Eq. (9), we obtain

$$(B_r^t + iB_z^t) = B_s^{ex}\varepsilon_t i[I_1(2\alpha\rho)e^{-i\phi}e^{-i\omega_w t} - I_3(2\alpha\rho)e^{3i\phi}e^{i\omega_w t}]. \tag{15}$$

In addition to the torsatron field, the betatron field contributes to the last term of Eq. (7). Assuming that the betatron field components vary as

$$B_r^b \approx -B_{z0}\frac{nz}{r_0},$$

$$B_z^b \approx B_{z0}\left[1 - \frac{n(r-r_0)}{r_0}\right],$$

we obtain

$$(B_r^b + iB_z^b) = iB_{z0}\left[1 + n - \frac{n}{r_0}(r - iz)\right], \tag{16}$$

where B_{z0} is the betatron field on the minor axis and n is the external field index.

2.2. Image Fields at the Ring Centroid

An accurate self-consistent determination of self-fields of a high-current electron ring in a modified betatron configuration that is supplemented by strong focusing is very difficult, because the minor cross section of the ring varies along the toroidal direction.

However, here we are interested in the macroscopic motion of the ring and therefore in the image fields that act on the ring centroid. These fields are not sensitive to the detailed shape of the ring cross section and thus can be computed approximately by assuming that the ring has a circular cross section that is uniformly filled. Neglecting toroidal corrections, the fields at the reference particle are

$$B_\phi = \frac{2en_0 v_\theta \pi r_b^2 \rho}{a^2 c(1 - \rho^2/a^2)}, \tag{17a}$$

$$E_\rho = -\frac{2en_0 \pi r_b^2 \rho}{a^2(1 - \rho^2/a^2)}, \tag{17b}$$

where r_b is the minor radius of the ring, a is the minor radius of the perfectly conducting torus, and n_0 is the uniform electron density. The fields given by Eqs. (17a) and (17b) are for a straight, cylindrical beam. The toroidal corrections are addressed in the next section.

Since

$$B_r = -B_\phi \sin\phi,\ E_r = E_\rho \cos\phi, \tag{18a}$$

and

$$B_z = B_\phi \cos\phi, E_z = E_\rho \sin\phi, \tag{18b}$$

Eqs. (17) and (18) give

$$-\frac{e}{m}[(E_r + iE_z) - i\beta_\theta(B_r + iB_z)] = \frac{\omega_p^2}{2}\left(\frac{r_b}{a}\right)^2 \frac{X + \delta r + i(Z + \delta z)}{(1 - \rho^2/a^2)\gamma^2}, \tag{19}$$

where ω_p is the ring plasma frequency, i.e., $\omega_p^2 = 4\pi e^2 n_0/m$, and $\beta_\theta = v_\theta/c \approx \beta = v/c$.

2.3. *Taylor Series Expansion of the Fields*

To separate the slow from the fast motion of the reference electron, it is necessary to expand the fields as a Taylor series about the guiding center.[26] Neglecting terms higher than quadratic, we have

$$B(r, z) \cong B(R, \Phi) + \boldsymbol{\delta\rho} \cdot \boldsymbol{\nabla} B|_{R,\Phi} = B(R, \Phi) + \tfrac{1}{2}(\delta u + \delta u^*)\frac{\partial B}{\partial X} + \frac{1}{2i}(\delta u - \delta u^*)\frac{\partial B}{\partial Z}. \tag{20}$$

Since

$$X = R\cos\Phi \quad \text{and} \quad Z = R\sin\Phi,$$

$$\frac{\partial}{\partial R} = \frac{\partial X}{\partial R}\frac{\partial}{\partial X} + \frac{\partial Z}{\partial R}\frac{\partial}{\partial Z} = \cos\Phi\frac{\partial}{\partial X} + \sin\Phi\frac{\partial}{\partial Z},$$

and

$$\frac{\partial}{\partial \Phi} = \frac{\partial X}{\partial \Phi}\frac{\partial}{\partial X} + \frac{\partial Z}{\partial \Phi}\frac{\partial}{\partial Z} = -R\sin\Phi\frac{\partial}{\partial X} + R\cos\Phi\frac{\partial}{\partial Z},$$

Equation (20) becomes

$$B(r, z) \cong B(R, \Phi) + \tfrac{1}{2}\delta u e^{-i\Phi}\left(\frac{\partial}{\partial R} - \frac{i}{R}\frac{\partial}{\partial \Phi}\right)B + \tfrac{1}{2}\delta u^* e^{i\Phi}\left(\frac{\partial}{\partial R} + \frac{i}{R}\frac{\partial}{\partial \Phi}\right)B. \tag{21}$$

Furthermore, we shall assume that the reference electron rotates around the guiding center with frequency $\pm\omega_w$, i.e.,

$$\delta u = \delta u_+ e^{i\omega_w t} + \delta u_- e^{-i\omega_w t}. \tag{22}$$

This assumption is supported by the following two observations. We have shown[24] that, when $\omega_w \ll \Omega_\theta/\gamma$, ω_w is an eigenfrequency of the linear system and that

$$\omega_w \gg \omega_s \equiv (\Omega_s^{ex}\varepsilon_t/\gamma)^2/[4(1 - \hat{\Omega}_\theta/\gamma\omega_w)(\hat{\Omega}_\theta/\gamma)],$$

where ω_s is the slowest eigenmode of the linear system,

$$\Omega_s^{ex} = eB_s^{ex}/mc = \Omega_{s0}^{ex} r_0/(r_0 + X),$$

$$\Omega_0 = eB_0/mc, \quad \text{and} \quad \hat{\Omega}_\theta = -(\Omega_0 + \Omega_s^{ex}).$$

In addition, extensive numerical results show that, when $\omega_w \ll \Omega_\theta/\gamma$, the electrons gyrate around the guiding center at a frequency ω_w.

The time derivative of Eq. (22) is

$$\delta\dot{u} = i\omega_w(\delta u_+ e^{i\omega_w t} - \delta u_- e^{-i\omega_w t}) + \dot{\mathbf{R}} \cdot \nabla(\delta u_+ e^{i\omega_w t} + \delta u_- e^{-i\omega_w t}). \tag{23}$$

We will show later that $\delta u_+ \sim I_3(2\alpha\rho)$ and $\delta u_- \sim I_1(2\alpha\rho)$, and therefore that $\nabla\delta u_\pm \sim 2\alpha\delta u_\pm$. The second term in Eq. (23) can be neglected, provided

$$\begin{aligned} &\dot{\mathbf{R}} \cdot \nabla\delta u_\pm \ll \omega_w \delta u_\pm, \quad \text{or} \\ &\dot{U} \ll v_\theta. \end{aligned} \tag{24}$$

2.4. *Time-Averaged Equations*

By substituting the Taylor-expanded fields of Eqs. (10), (15), (16), and (19) into Eq. (7), using Eq. (21), omitting terms quadratic in δu, multiplying the resulting equation by $e^{im\omega_w t}$, taking the time average from 0 to $2\pi/\omega_w$, and omitting the small term $\langle \ddot{U} e^{im\omega_w t}\rangle$, we obtain the following expression for $m = 0$:

$$\begin{aligned} &\frac{\dot{\gamma}}{\gamma}\dot{U} - \frac{i\dot{U}}{\gamma}\left(\Omega_0 + \frac{\Omega_{s0}^{\mathrm{ex}} r_0}{r_0 + X}\right) + i\frac{v_\theta \alpha}{\gamma}\Omega_s^{\mathrm{ex}}\varepsilon_t\left(\frac{\dot{U}}{v_\theta} f_1 - if_2\right)\delta u_- + \frac{iv_\theta}{\gamma}\alpha\Omega_s^{\mathrm{ex}}\varepsilon_t\left(\frac{\dot{U}}{v_\theta} f_3^* + if_2^*\right)\delta u_+ \\ &\quad + \frac{iv_\theta \alpha}{\gamma}\Omega_s^{\mathrm{ex}}\varepsilon_t\left(\frac{\dot{U}}{v_\theta} f_1^* - if_0\right)\delta u_-^* + \frac{iv_\theta \alpha}{\gamma}\Omega_s^{\mathrm{ex}}\varepsilon_t\left(\frac{\dot{U}}{v_\theta} f_3 + if_4\right)\delta u_+^* \\ &\quad = \frac{\omega_p^2}{2}\left(\frac{r_b^2}{a}\right)\frac{(X + iZ)}{(1 - R^2/a^2)\gamma^3} + \frac{v_\theta^2}{r_0 + X} - \left(\frac{v_\theta}{\gamma}\right)\Omega_{z0}\left(1 - \frac{n}{r_0}(X - iZ)\right], \end{aligned} \tag{25}$$

where

$$f_n(R, \Phi) = I_n(2\alpha R)e^{in\Phi}.$$

In addition, for $m = 1$ the time-averaged equation is

$$\begin{aligned} &-\omega_w\Bigg[\omega_w + \frac{\dot{\gamma}}{\gamma}i + \frac{1}{\gamma}\left(\Omega_0 + \frac{\Omega_{s0}^{\mathrm{ex}} r_0}{r_0 + X}\right) - \underline{\frac{i\dot{U}}{2\gamma\omega_w}\frac{\Omega_{s0}^{\mathrm{ex}} r_0}{(r_0 + X)^2}} \\ &\quad - \underline{\frac{v_\theta^2}{2(r_0 + X)^2\omega_w}} + \frac{1}{2}\frac{\omega_p^2}{\gamma^3\omega_w}\left(\frac{r_b}{a}\right)^2\frac{1}{(1 - R^2/a^2)^2}\Bigg]\delta u_- \\ &\quad - \Bigg[\frac{v_\theta}{\gamma}\frac{n}{r_0}\Omega_{z0} + \underline{\frac{1}{2}\frac{\omega_p^2}{\gamma^3}\left(\frac{r_b}{a}\right)^2\frac{\left(\frac{X}{a} + i\frac{Z}{a}\right)^2}{(1 - R^2/a^2)^2}} - \underline{\frac{i\dot{U}}{2\gamma}\frac{\Omega_{s0}^{\mathrm{ex}} r_0}{(r_0 + X)^2}} - \underline{\frac{v_\theta^2}{2(r_0 + X)^2}}\Bigg]\delta u_+^* \\ &\quad = -\frac{\Omega_s^{\mathrm{ex}}\varepsilon_t}{\gamma}(v_\theta f_1^* + i\dot{U}f_2^*). \end{aligned} \tag{26}$$

Similarly, for $m = -1$ the time-averaged equation gives

$$-\left(\frac{v_\theta}{\gamma}\frac{n}{r_0}\Omega_{z0}+\frac{1}{2}\frac{\omega_p^2}{\gamma_3}\left(\frac{r_b}{a}\right)^2\frac{\left(\frac{X}{a}+i\frac{Z}{a}\right)^2}{(1-R^2/a^2)^2}-\frac{v_\theta^2}{2(r_0+X)^2}\right.$$
$$\left.-\frac{i\dot{U}}{2\gamma}\frac{\Omega_{s0}^{ex}r_0}{(r_0+X)^2}\right)\delta u_-^* - \omega_w\left(\omega_w-\frac{\dot{\gamma}}{\gamma}i\right.$$
$$-\frac{i\dot{U}}{2\gamma\omega_w}\frac{\Omega_{s0}^{ex}r_0}{(r_0+X)^2}-\frac{v_\theta^2}{2(r_0+X)^2\omega_w}+\frac{\omega_p^2}{2\omega_w\gamma^3}\left(\frac{r_b}{a}\right)^2$$
$$\left.\times\frac{1}{(1-R^2/a^2)^2}-\frac{1}{\gamma}\left(\Omega_0+\frac{\Omega_{s0}^{ex}r_0}{r_0+X}\right)\right)\delta u_+$$
$$=\frac{v_\theta}{\gamma}\Omega_s^{ex}\varepsilon_t f_3-\frac{i\dot{U}}{\gamma}\Omega_s^{ex}\varepsilon_t f_2. \tag{27}$$

For the parameters of interest, the underlined terms in Eqs. (26) and (27) are small in comparison with the non-underlined terms and can therefore be omitted.

In addition, assuming that $\dot{\gamma}/\gamma \ll \omega_w$, Eqs. (26) and (27) give

$$\delta u_- = \frac{(v_\theta/\gamma)^2\frac{n}{r_0}\Omega_{z0}\Omega_s^{ex}\varepsilon_t f_3^* + f_1(v_\theta/\gamma)\Omega_s^{ex}\varepsilon_t\omega_w(\Omega_w+\hat{\Omega}_\theta/\gamma)}{\omega_w^2(\Omega_w^2-\hat{\Omega}_\theta^2/\gamma^2)}$$
$$\cong\frac{f_1^*(v_\theta/\gamma)\Omega_s^{ex}e_t}{\omega_w(\Omega_w-\hat{\Omega}_\theta/\gamma)}, \tag{28}$$

and

$$\delta u_+^* = \frac{-(v_\theta/\gamma)\Omega_s^{ex}\varepsilon_t(f_3^*\omega_w(\Omega_w-\hat{\Omega}_\theta/\gamma)+f_1^*(v_\theta/\gamma)\Omega_{z0}n/r_0)}{\omega_w^2(\Omega_w^2-\hat{\Omega}_\theta^2/\gamma^2)-\left(\frac{v_\theta n}{r_0}\frac{\Omega_{z0}}{\gamma}\right)^2}$$
$$\approx -\frac{(v_\theta/\gamma)\Omega_s^{ex}\varepsilon_t f_3^*}{\omega_w(\Omega_w+\hat{\Omega}_\theta/\gamma)}, \tag{29}$$

where

$$\Omega_w = \omega_w+\frac{1}{2}\frac{\omega_p^2}{\gamma^3\omega_w}\left(\frac{r_b}{a}\right)^2\frac{1}{(1-R^2/a^2)^2}\cong\omega_w$$

and

$$\hat{\Omega}_\theta = -\left(\Omega_0+\frac{\Omega_{s0}^{ex}r_0}{r_0+X}\right).$$

Substituting $\delta u_\pm$ from Eqs. (28) and (29) into the equation for the slow motion

[Eq. (25)], we obtain

$$\dot{Z} + \frac{v_\theta(\Omega_s^{ex}\varepsilon_t/\gamma)^2[I_2(2\alpha R) + I_0(2\alpha R)]I_1(2\alpha R)X}{2(\hat{\Omega}_\theta/\gamma)(\hat{\Omega}_\theta/\gamma - \Omega_w)R} - \frac{v_\theta(\Omega_s^{ex}\varepsilon_t/\gamma)^2[I_2(2\alpha R) + I_4(2\alpha R)]I_3(2\alpha R)X}{2(\hat{\Omega}_\theta/\gamma)(\hat{\Omega}_\theta/\gamma + \Omega_w)R}$$

$$= -\frac{v_\theta^2}{(\hat{\Omega}_\theta/\gamma)(r_0 + X)} + \frac{v_\theta(\Omega_{z0}/\gamma)}{(\hat{\Omega}_\theta/\gamma)}\left(1 - \frac{n}{r_0}X\right) - \frac{\omega_p^2}{2(\hat{\Omega}_\theta/\gamma)}\left(\frac{r_b}{a}\right)^2 \frac{X}{(1 - R^2/a^2)\gamma^3}, \quad (30)$$

and

$$\dot{X} - \frac{v_\theta(\Omega_s^{ex}\varepsilon_t/\gamma)^2[I_2(2\alpha R) + I_0(2\alpha R))I_1(2\alpha R)Z}{2(\hat{\Omega}_\theta/\gamma)(\hat{\Omega}/\gamma - \Omega_w)R} + \frac{v_\theta(\Omega_s^{ex}\varepsilon_t/\gamma)^2[I_2(2\alpha R) + I_4(2\alpha R)]I_3(2\alpha R)Z}{2(\hat{\Omega}_\theta/\gamma)(\hat{\Omega}_\theta/\gamma + \Omega_w)R}$$

$$= -\frac{nv_\theta(\Omega_{z0}/\gamma)}{(\hat{\Omega}_\theta/\gamma)}\frac{Z}{r_0} + \frac{\omega_p^2}{2(\hat{\Omega}_\theta/\gamma)}\left(\frac{r_b}{a}\right)^2 \frac{Z}{(1 - R^2/a^2)\gamma^3}. \quad (31)$$

These are the nonlinear equations that describe the guiding-center (slow) motion of the beam centroid. They have been derived under the assumption that γ changes very little in the time scale of ω_w, i.e., $\dot{\gamma}/\gamma \ll \omega_w$. Since the variation of γ is mainly due to space charge, this condition can be written

$$\frac{\nu}{\gamma}\frac{R}{a}\frac{\delta\rho}{a} \ll \frac{\pi}{2}, \quad (32)$$

where ν is the Budker parameter and $\delta\rho$ is the amplitude of the motion associated with ω_w. The inequality of Eq. (32) is easily satisfied because $\nu/\gamma \ll 1$, $\delta\rho/a \ll 1$, and $R/a < 1$. In contrast, the variation of γ on a slow time scale cannot be neglected in the presence of space charge. This is discussed in the next section.

2.5. Toroidal Corrections

So far, we have made the assumption that the aspect ratio a/r_0 is very small; thus, all the toroidal corrections associated with the fields have been neglected.

For devices with parameters similar to those listed in Table I, the toroidal corrections associated with the torsatron fields change the ring orbits only slightly, provided that the net vertical field of the unidirectional torsatron windings is canceled with outboard coils. Even with the torsatron field toroidal corrections, we were able to derive the two slow equations of motion, but we were unable to analytically integrate them and thus to derive a constant of the motion.

The toroidal corrections of the self-fields become very important when the ring current reaches a few kiloamperes. In addition to changing the speed of rotation

around the equilibrium position, the self-field toroidal corrections modify the value of the vertical field required to confine the beam at its equilibrium position.

To lowest order, the self-field toroidal corrections can be included in the slow equations of motion by replacing the fields of Eqs. (17) and (18) by[6]

$$E_r = -(2|e|N_l/a)\left[\frac{X}{a} + \frac{a}{2(r_0+X)}\ln\frac{a}{r_b} + \frac{r_b^2}{8(r_0+X)a}\right], \tag{33a}$$

$$E_z = -(2|e|N_l/a)(Z/a), \tag{33b}$$

$$E_\theta = -(2|e|N_l\beta_\theta/c)\left[\frac{X\dot{X}+Z\dot{Z}}{a^2} - \frac{\dot{X}}{2(r_0+X)}\ln\frac{a}{r_b} - \frac{2\nu}{\gamma^3}\left(1+\frac{1}{\beta_\theta^2}\right)\left(\frac{X\dot{X}+Z\dot{Z}}{a^2}\right)\left(\frac{1}{2}+\ln\frac{a}{r_b}\right)\right], \tag{33c}$$

$$B_r = -(2|e|N_l\beta_\theta/a)(Z/a), \tag{33d}$$

and

$$B_z = (2|e|N_l\beta_\theta/a)\left[\frac{X}{a} - \left(\frac{a}{2(r_0+X)}\right)\left(\ln\frac{a}{r_b}+1\right) + \frac{r_b^2}{8(r_0+X)a}\right], \tag{33e}$$

where N_l is the number of electrons per unit length. These fields modify only the last term of Eqs. (30) and (31). The nonlinear equations that describe the slow motion of the beam centroid now become

$$\begin{aligned}
&\ddot{Z} + \frac{v_\theta(\Omega_s^{ex}\varepsilon_t/\gamma)^2}{2(\hat{\Omega}_\theta/\gamma)} \\
&\quad\times\left\{\frac{[I_2(2\alpha R)+I_0(2\alpha R)]I_1(2\alpha R)}{(\hat{\Omega}_\theta/\gamma-\Omega_w)} - \frac{[I_2(2\alpha R)+I_4(2\alpha R)]I_3(2\alpha R)}{(\hat{\Omega}_\theta/\gamma+\Omega_w)}\right\}\left(\frac{X}{R}\right) \\
&= -\frac{v_\theta^2}{(\hat{\Omega}_\theta/\gamma)(r_0+X)} + \frac{v_\theta(\Omega_{z0}/\gamma)}{(\hat{\Omega}_\theta/\gamma)}\left(1-\frac{n}{r_0}X\right) \\
&\qquad - \frac{\omega_p^2}{2(\hat{\Omega}_\theta/\gamma)}\left(\frac{r_b}{a}\right)^2\left\{\frac{X}{\gamma^3} + \frac{a^2}{2\gamma(r_0+X)}\left[\beta_\theta^2 + (1+\beta_\theta^2)\ln\frac{a}{r_b}\right]\right\},
\end{aligned} \tag{34}$$

$$\begin{aligned}
&\ddot{X} - \frac{v_\theta(\Omega_s^{ex}\varepsilon_t/\gamma)^2}{2(\hat{\Omega}_\theta/\gamma)} \\
&\quad\times\left\{\frac{[I_2(2\alpha R)+I_0(2\alpha R)]I_1(2\alpha R)}{(\hat{\Omega}_\theta/\gamma-\Omega_w)} - \frac{[I_2(2\alpha R)+I_4(2\alpha R)]I_3(2\alpha R)}{(\hat{\Omega}_\theta/\gamma+\Omega_w)}\right\}\left(\frac{Z}{R}\right) \\
&= -\frac{nv_\theta(\Omega_{z0}/\gamma)}{(\hat{\Omega}_\theta/\gamma)}\frac{Z}{r_0} + \frac{\omega_p^2}{2(\hat{\Omega}_\theta/\gamma)}\left(\frac{r_b}{a}\right)^2\frac{Z}{\gamma^3},
\end{aligned} \tag{35}$$

and

$$\begin{aligned}
\frac{d\gamma}{dt}\left[1+\frac{2\nu}{\gamma^3}\left(\frac{1}{2}+\ln\frac{a}{r_b}\right)\right] = 2\nu\left\{\frac{d}{dt}\left[\frac{X^2+Z^2}{a^2} + (r_b^2/8a^2)\ln\frac{(r_0+X)}{r_0}\right]\right. \\
\left. -(1/\gamma^2)\frac{d}{dt}\left[\frac{X^2+Z^2}{2a^2} - \frac{1}{2}\ln\frac{a}{r_b}\ln\frac{(r_0+X)}{r_0}\right]\right\}.
\end{aligned} \tag{36}$$

TABLE I

Parameters of The Runs Shown in Fig. 2

Torus major radius, r_0 (cm)	100
Winding minor radius, ρ_0 (cm)	18
Toroidal chamber minor radius, a (cm)	20
$\alpha = 2\pi/L$ (cm^{-1})	0.1
Field strength factor, ε_t	−0.04275
Winding current, I (kA)	25
l	2
Torsatron toroidal field, B_s (kG)	1.0
Additional toroidal field, B_s^{ex} (kG)	3.0
Betatron field, B_{z0} (G)	35
External field index, n	0.5
Beam electron density, n_0 (cm^{-3})	0
Initial γ	2.96
Beam minor radius, r_b (cm)	1.0
B_{z0} (G) to hold beam at r_0	47.27

Equation (36) describes the variation of γ as the ring moves along its slow orbit. In addition to the effect of E_r and E_z, Eq. (36) includes the effect of the toroidal electric field that is generated by the time-varying self-magnetic vector potential as the beam centroid moves in the transverse plane.

The guiding center of the electron ring gyrates around the equilibrium position X_{eq}, which can be determined from Eqs. (34) and (35) by taking $\dot{X} = \dot{Z} = 0$ and is given by the expression

$$
\begin{aligned}
&-\frac{(\Omega_s^{ex}\varepsilon_t/\gamma)^2}{2(\Omega_{z0}/\gamma)} \\
&\times\left\{\frac{[I_0(2\alpha X_{eq})+I_2(2\alpha X_{eq})]I_1(2\alpha X_{eq})}{\left[\dfrac{\Omega_0}{\gamma}+\dfrac{\Omega_{s0}^{ex}r_0}{\gamma(r_0+X_{eq})}+\Omega_w\right]}-\frac{[I_2(2\alpha X_{eq})+I_4(2\alpha X_{eq})]I_3(2\alpha X_{eq})}{\left[\Omega_0/\gamma+\dfrac{\Omega_{s0}^{ex}r_0}{\gamma(r_0+X_{eq})}-\Omega_w\right]}\right\} \\
&=-\frac{v_\theta}{(r_0+X_{eq})(\Omega_{z0}/\gamma)}+\left(1-\frac{n}{r_0}X_{eq}\right) \\
&\quad-\frac{\omega_p^2}{2(\Omega_{z0}/\gamma)}\left(\frac{r_b}{a}\right)^2\frac{1}{v_\theta}\left\{\frac{X_{eq}}{\gamma^3}+\frac{a^2}{2\gamma(r_0+X_{eq})}\left[\beta_\theta^2+(1+\beta_\theta^2)\ln\frac{a}{r_b}\right]\right\}. \qquad (37)
\end{aligned}
$$

When the electron ring is located at its equilibrium position, γ does not vary with time. However, when the injection position is different from the equilibrium position, the energy of the reference particle is different in these two locations and can be found by integrating Eq. (36), which gives

$$
\begin{aligned}
&\gamma+2\nu\left[\frac{1}{2}+\ln\frac{a}{r_b}-\frac{X^2+Z^2}{a^2}-\frac{r_b^2}{8a^2}\frac{X}{(r_0+X)}\right] \\
&\qquad-\frac{\nu}{\gamma^2}\left[\frac{1}{2}+\ln\frac{a}{r_b}-\frac{X^2+Z^2}{a^2}+\ln\frac{a}{r_b}\ln\frac{(r_0+X)}{r_0}\right]=\gamma_c, \qquad (38)
\end{aligned}
$$

where γ_c is a constant that is determined from the injection conditions. Equation (38) has been derived under the assumption that $\gamma_\theta \cong \gamma$, and a small term proportional to ν/γ^3 has been omitted.

2.6. *Integration of Nonlinear Equations*

The nonlinear Eqs. (34) and (35) can be integrated, provided that the spatial variation of $\hat{\Omega}_\theta$ can be neglected, i.e., when $\hat{\Omega}_\theta = \hat{\Omega}_{\theta 0} = \text{constant}$.

Multiplying Eq. (34) by $\dot{X}$ and Eq. (35) by $\dot{Z}$ and taking their difference, we obtain

$$
\begin{aligned}
0 = & -\frac{v_\theta(\Omega_s^{ex}\varepsilon_t/\gamma)^2[I_0(2\alpha R)+I_2(2\alpha R)]I_1(2\alpha R)}{2(\hat{\Omega}_{\theta 0}/\gamma)(\hat{\Omega}_{\theta 0}/\gamma-\Omega_w)R}\frac{1}{2}\frac{d}{dt}(R^2) \\
& +\frac{v_\theta(\Omega_s^{ex}\varepsilon_t/\gamma)^2[I_2(2\alpha R)+I_4(2\alpha R)]I_3(2\alpha R)}{2(\hat{\Omega}_{\theta 0}/\gamma)(\hat{\Omega}_0/\gamma+\Omega_w)R}\frac{1}{2}\frac{d}{dt}(R^2)-\frac{\omega_p^2}{2(\hat{\Omega}_{\theta 0}/\gamma)}\left(\frac{r_b}{a}\right)^2 \\
& \times\left\{\frac{\frac{1}{2}\frac{d}{dt}(X^2+Z^2)}{\gamma^3}+\frac{a^2\dot{X}}{2\gamma(r_0+X)}\left[\beta_\theta^2+(1+\beta_\theta^2)\ln\frac{a}{r_b}\right]\right\} \\
& -\frac{v_\theta^2}{(\hat{\Omega}_{\theta 0}/\gamma)}\frac{d}{dt}\ln(1+X/r_0)+\frac{v_\theta(\Omega_{z0}/\gamma)}{(\hat{\Omega}_{\theta 0}/\gamma)}\frac{d}{dt}\left(X-\frac{n}{2r_0}X^2\right) \\
& +\frac{(v_\theta/\gamma)\Omega_{z0}}{2(\hat{\Omega}_{\theta 0}/\gamma)}\frac{n}{r_0}\frac{d}{dt}(Z^2). \qquad (39)
\end{aligned}
$$

Before acceleration and for the parameters of interest $\Omega_w \cong \omega_w \ll \hat{\Omega}_{\theta 0}/\gamma$ and therefore Ω_w can be omitted. With this approximation, the first two terms of Eq. (39) become independent of γ, and they can be written as a total time derivative. Let

$$
[I_0(2\alpha R)+I_2(2\alpha R)]I_1(2\alpha R) \equiv \frac{d\psi_1}{dR},
$$

where ψ_1 is a function to be determined.

Since

$$
\frac{d\psi_1}{dt}=\frac{d\psi_1}{dR}\frac{dR}{dt}=(I_0+I_2)I_1\frac{dR}{dt}, \qquad (40)
$$

the function ψ_1 is obtained from

$$
\psi_1=\int I_0(2\alpha R)I_1(2\alpha R)\,dR+\int I_2(2\alpha R)I_1(2\alpha R)\,dR=\frac{I_1^2}{2\alpha}. \qquad (41)
$$

Similarly, the second term gives

$$
\psi_2=\int I_2(2\alpha R)I_3(2\alpha R)\,dR+\int I_4(2\alpha R)I_3(2\alpha R)\,dR=I_3^2/2\alpha. \qquad (42)
$$

Since the two torsatron terms do not include toroidal corrections, the factor X/r_0 is omitted when it appears in these terms. With this approximation, Eq. (36) together with Eqs. (39) through (42) give

$$\frac{d}{dt}\Bigg\{(r_0+X)\beta_\theta\gamma+\frac{(\Omega_s^{ex}\varepsilon_t)^2}{4c\alpha\hat{\Omega}_{\theta 0}}r_0[I_1^2(2\alpha R)-I_3^2(2\alpha R)] - \frac{\Omega_{z0}r_0}{c}(r_0+X)\left[1+(1-n)\frac{X^2}{2r_0^2}+\frac{nZ^2}{2r_0^2}\right] + 2\nu/\beta_\theta(r_0+X)\left(1/2+\ln\frac{a}{r_b}-\frac{X^2+Z^2}{a^2}-\frac{r_b^2}{8a^2}\frac{X}{r_0}\right)\Bigg\}=0. \quad (43)$$

Equation (43) can be expressed in a different form that is very revealing. Defining a stream function

$$\psi=(r_0+X)[A_\theta^{tors}+A_\theta^{bet}+A_\theta^{self}],$$

where

$$A_\theta^{tors}=-B_s^{ex}\varepsilon_t^2\frac{\Omega_s^{ex}}{4\alpha\hat{\Omega}_{\theta 0}}\frac{r_0}{(r_0+X)}[I_1^2(2\alpha R)-I_3^2(2\alpha R)],$$

$$A_\theta^{bet}=B_{z0}r_0\left[1+(1-n)\frac{X^2}{2r_0^2}+\frac{nZ^2}{2r_0^2}\right],$$

and

$$A_\theta^{self}=-2N_\ell|e|\beta_\theta\left(1/2+\ln\frac{a}{r_b}-\frac{X^2+Z^2}{a^2}-\frac{r_b^2}{8a^2}\frac{X}{r_0}\right),$$

Eq. (43) becomes

$$(r_0+X)\beta_\theta\gamma-\frac{|e|}{mc^2}\psi=\frac{\langle P_\theta\rangle}{mc}=\text{constant} \quad (44)$$

or

$$(r_0+X)\Bigg\{\beta_\theta\left[\gamma+2\nu\left(1/2+\ln\frac{a}{r_b}-\frac{X^2+Z^2}{a^2}-\frac{r_b^2}{8a^2}\frac{X}{r_0}\right)\right] - \frac{\Omega_{z0}r_0}{c}\left[1+(1-n)\frac{X^2}{2r_0^2}+n\frac{Z^2}{2r_0^2}\right]+\frac{(\Omega_s^{ex}\varepsilon_t)^2}{4\alpha c\hat{\Omega}_{\theta 0}}\frac{r_0}{(r_0+X)}[I_1^2(2\alpha R)-I_3^2(2\alpha R)]\Bigg\} =\frac{\langle P_\theta\rangle}{mc}=K. \quad (45)$$

According to Eq. (44), the averaged (over the fast motion) canonical momentum of the reference electron is approximately conserved.

The equation that describes the nonlinear slow orbits of the beam centroid in the plane transverse to the minor axis can be found by combining Eqs. (38) and (45). When $\varepsilon_t=0$, i.e., for the modified betatron, P_θ is an exact constant of the motion, and Eq. (45) accurately predicts the macroscopic beam orbits. In the presence of strong focusing, i.e., when $\varepsilon_t\neq 0$, A_θ^{tors} is known only approximately,

and thus the predictions of Eq. (45) are less accurate. In the latter case, the error in $\langle P_\theta \rangle / mc$ is proportional to $(\Omega_s^{ex}\varepsilon_t)^2 R$.

According to Eq. (45), the orbits pass through the minor axis when the reference electron is injected into the device with a $\langle P_\theta \rangle = \langle P_\theta \rangle_0$ that satisfies the relation

$$\frac{r_0\Omega_{z0}}{c} - \left[1 + \frac{2\nu}{\gamma_0}\left(1/2 + \ln\frac{a}{r_b}\right)\right]\beta_{\theta 0}\gamma_0 = -\frac{\langle P_\theta \rangle_0}{mcr_0}. \tag{46}$$

In addition, Eqs. (37) and (46) predict that the equilibrium position of the reference electron will be located on the minor axis when its averaged canonical momentum satisfies the relation

$$\frac{\langle P_\theta \rangle_{00}}{mcr_0} = -(\nu/\gamma_0^2\beta_{\theta 0}) \ln\frac{a}{r_b}.$$

Near the minor axis, i.e., when $2\alpha R \ll 1$ and $X/r_0 \ll 1$, Eq. (45) can be linearized, and the resulting expression, when the small term that contains I_3 is omitted, is

$$\begin{aligned}
&\left[\frac{\Omega_{z0}r_0}{2c}(1-n) - \frac{(\Omega_s^{ex}\varepsilon_t)^2\alpha r_0^2}{4c\hat{\Omega}_{\theta 0}} - \frac{\nu r_0^2}{\gamma_0^2 a^2 \beta_{\theta 0}} + \frac{\langle P_\theta \rangle}{mcr_0}\right]\left(\frac{X}{r_0}\right)^2 \\
&+ \left[\frac{\Omega_{z0}r_0}{2c}n - \frac{(\Omega_s^{ex}\varepsilon_t)^2\alpha r_0^2}{4c\hat{\Omega}_{\theta 0}} - \frac{\nu r_0^2}{\gamma_0^2 a^2 \beta_{\theta 0}}\right]\left(\frac{Z}{r_0}\right)^2 \\
&- \left[\frac{\langle P_\theta \rangle}{mcr_0} + \frac{\nu}{2\gamma_0^2\beta_{\theta 0}}\left(2\ln\frac{a}{r_b} + \frac{r_b^2}{2a^2}\right)\right]\left(\frac{X}{r_0}\right) = -\frac{\delta P_\theta}{mcr_0},
\end{aligned} \tag{47}$$

where

$$\frac{\delta P_\theta}{mcr_0} = \frac{\langle P_\theta \rangle}{mcr_0} - \frac{\langle P_\theta \rangle_{00}}{mcr_0} = \frac{\langle P_\theta \rangle}{mcr_0} + \frac{\nu}{\gamma_0^2\beta_{\theta 0}} \ln\frac{a}{r_b}.$$

When $\varepsilon_t = 0$, Eq. (47) is very similar to Eq. (20) of Ref. 6. The small differences in the two orbit equations are probably associated with the different approximations used to compute γ. In general,

$$\frac{d\gamma}{dt} = \frac{e}{mc^2}\left(\frac{d\phi}{dt} - \frac{1}{\gamma^2}\frac{\partial\phi}{\partial t}\right), \tag{48}$$

where ϕ is the electrostatic potential at the ring centroid. In addition to keeping the first term in Eq. (48), as in Ref. 6, Eq. (36) includes the most important contributions from the second term of Eq. (48).

Equation (45) is plotted in Fig. 2a for various values of constant $\langle P_\theta \rangle / mc$, for zero electron beam density. The parameters for the results of Fig. 2 are listed in Table I.

All the orbits close inside the vacuum chamber. However, those that lie less than a minor ring radius from the wall are not useful, because when the beam is moving along one of these orbits, it will scrape the wall. In addition, it should be noticed that the existence of drift surfaces for R near ρ_0 is certainly due to the

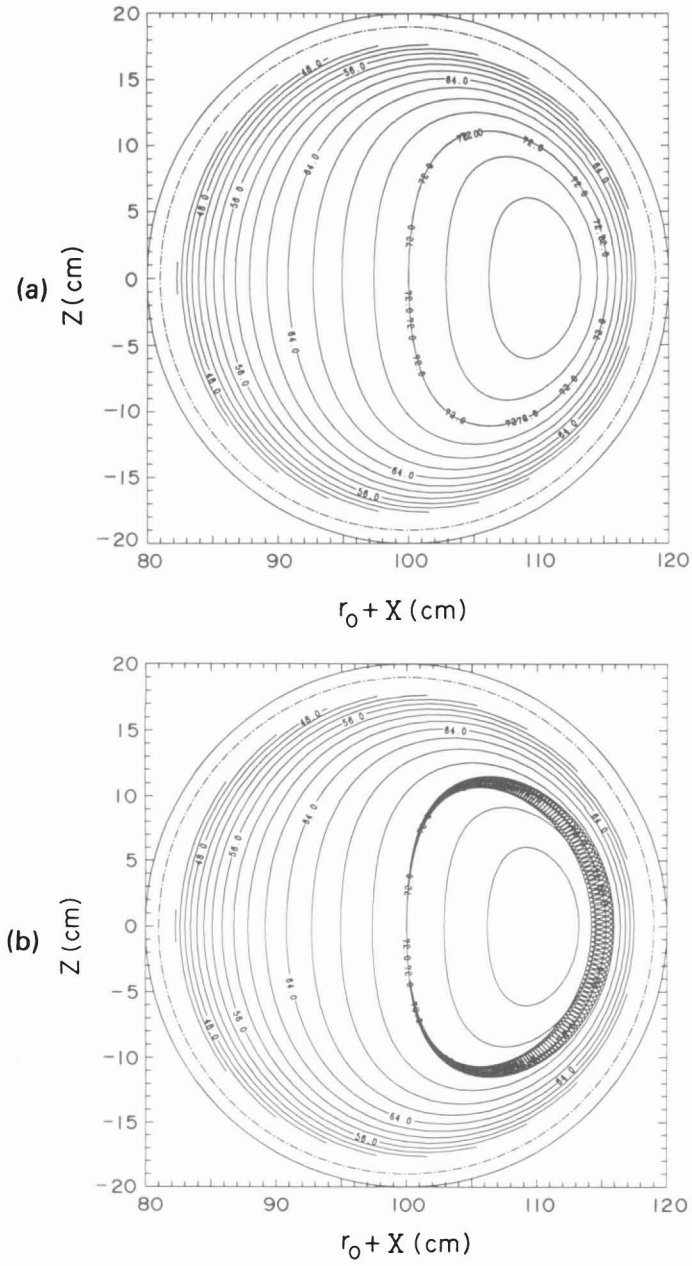

FIGURE 2 (a) Guiding-center orbits from Eq. (45) for several values of constant K for the parameters listed in Table I. (b) An electron beam orbit obtained from the numerical integration of orbit equations, superimposed on the $K = 72$ (cm) guiding-center orbit of (a). It is apparent that the constant of the motion accurately predicts the guiding-center motion. (c) Same as (b) but with the toroidal corrections of the torsatron field included in the numerical integration of the orbit equations. (d) Same as (a), but at a finer scale; (e) Values of $\langle P_\theta/mc \rangle$ along the symmetry plane ($Z = 0$). The equilibrium position coincides with the maximum of $\langle P_\theta/mc \rangle$.

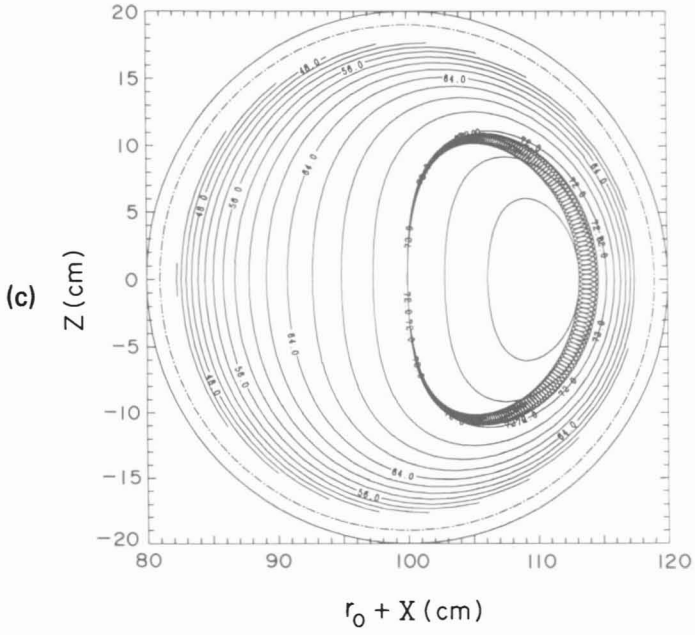

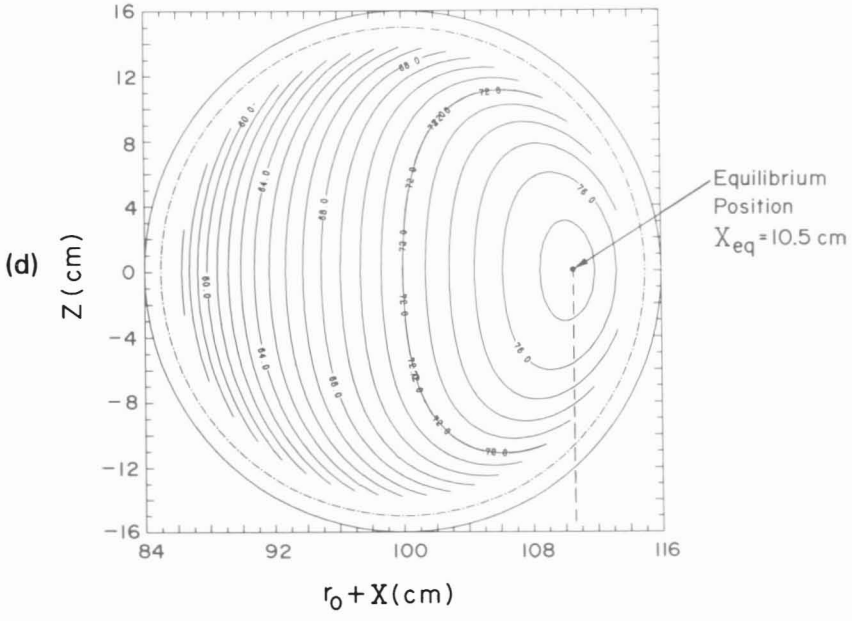

FIGURE 2 (*Continued*)

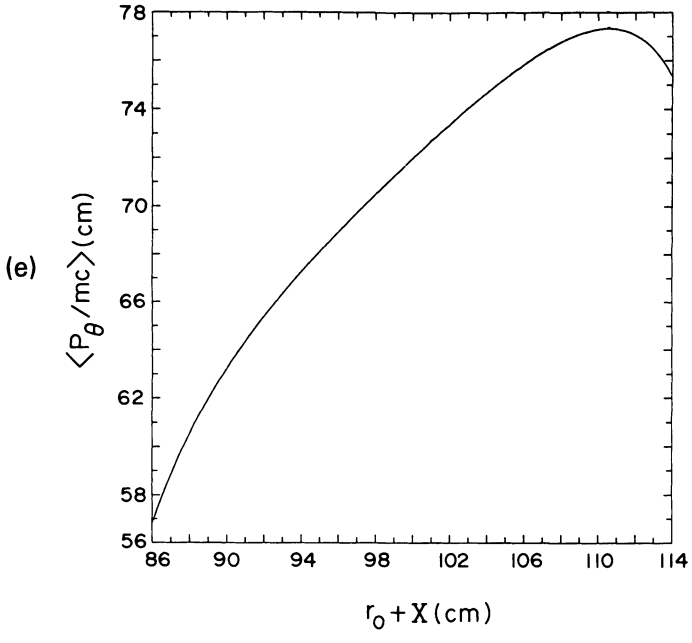

FIGURE 2 (*Continued*)

analytic approximation of the torsatron field. It is expected that the drift surfaces in an actual device near ρ_0 will be substantially different from those predicted by the analytic approximation.

Figure 2b shows an electron orbit obtained from the numerical integration of orbit equations, superimposed on a macroscopic orbit of Fig. 2a that corresponds to the same conditions. In both the numerically obtained orbit and the macroscopic orbit from the constant of the motion, the toroidal corrections of the torsatron field have been omitted. It is quite obvious that the constant of the motion accurately predicts the guiding-center motion. The period of the particle gyrating around the guiding center is about 1 ns, in agreement with Eq. (22), and the radius of fast gyration decreases as the electron moves toward the minor axis, in agreement with Eqs. (28) and (29).

The predictions of the constant of the motion remain rather accurate even when the toroidal corrections of the torsatron field are included in the orbit equations. Results are shown in Fig. 2c.

For the values of the parameters listed in Table I, Eq. (37) predicts that the nonlinear equilibrium position is located at $X_{eq} \cong 10.2$ cm. To determine accurately the equilibrium position, we have repeated the computer run of Fig. 2a using a finer scale. The results are shown in Fig. 2d and indicate an equilibrium position that is very close to 10.5 cm. This equilibrium position coincides with the maximum of the curve in Fig. 2e. To check these predictions, we made a computer run with the electron initially placed at $X = 10.0$ cm, $Z = 0$. We have observed that the electron started to gyrate around the $X = 10.25$ cm, $Z = 0$ point with a radius of a few millimetres. This test demonstrates unequivocally that Eq.

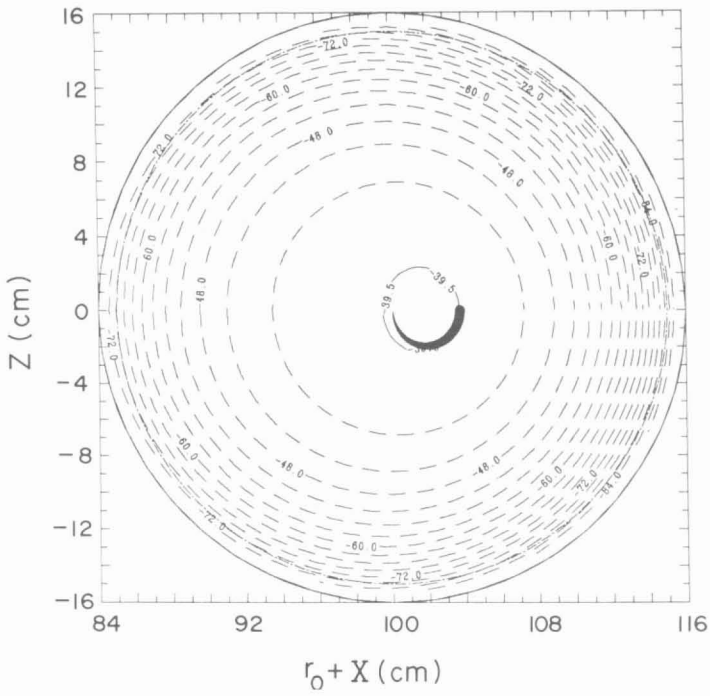

FIGURE 3 Part of an orbit obtained numerically from the exact equations of motion, superimposed on a guiding-center orbit (slow) that corresponds to the same conditions.

(37) accurately predicts the equilibrium position even when the parameter $2\alpha R > 1$. However, this is not the case with the linearized expression. For the parameters of Table I, the linear theory predicts that the equilibrium position is located in excess of 30 cm from the minor axis.

Figure 3 shows part of an orbit obtained from the numerical integration of the equation of motion, superimposed on a macroscopic orbit [from Eq. (45) with γ from Eq. (38)] that corresponds to the same conditions. The various parameters for this run are listed in Table II. The beam current is initially 4.659 kA and increases to 6 kA after acceleration, i.e., when $\beta_\theta \cong 1$. The agreement between the exact equations and the constant of the motion is satisfactory.

3. BEAM TRAPPING

The minimum requirements for trapping an electron beam in a toroidal device are:

(i) During the first revolution around the major axis, i.e., in a time $\tau \leqslant (2\pi/\Omega_{z0}/\gamma)$, the beam should drift along the guiding-center orbit a distance greater than $r_b + r_{\text{inj}}$, where r_b is the minor radius of the beam and r_{inj} is the injector radius.

TABLE II

Parameters of The Run Shown in Fig. 3

Torus major radius, r_0 (cm)		100
Winding minor radius, ρ_0 (cm)		18
Toroidal chamber minor radius, a (cm)		16
$\alpha = 2\pi L$ (cm^{-1})		0.06
Field strength factor, ε_t		−0.1698
Winding current, I (kA)		55
ℓ		2
Torsatron toroidal field, B_s (kG)		1.32
Additional toroidal field, B_s^{ex} (kG)		5.0
Betatron field, B_{z0} (G)		57
Equilibrium magnetic field at r_0, B_{eq} (G)		61.214
External field index, n		0.5
Electron beam current, I_b (kA)		4.659
Initial γ (at injection)		1.58
Diode γ_D		2.96
Minor beam radius, r_b (cm)		1.0
Initial positions (cm)	$X(t=0)$	3.75
	$Z(t=0)$	0
	$S(t=0)$	26.18
Initial velocities	$\dot{X}(t=0)$	0
	$\dot{Z}(t=0)$	0
	v_θ	0.774

(ii) In a bounce period τ_B, i.e., in the time the beam completes a revolution around the equilibrium position, the guiding-center orbit should be deformed radially near the injector at least as much as the distance $r_b + r_{inj}$.

(iii) Within a time interval of a few bounce periods, the beam should drift near the minor axis of the torus.

(iv) The radius of gyration around the guiding center should be substantially shorter than the radius of the guiding center.

The guiding center equations derived in the previous section provide a valuable guide in the development of a realistic trapping scheme for the following reasons. The beam drift velocity along the guiding-center orbit can be optimized using Eqs. (34) through (36). From the shape of the guiding-center orbit that can be determined from Eq. (45) and the bounce frequency, we can select the various parameters of the trapping field that will radially deform the guiding-center orbit by the desired amount so the beam will not strike the injector after a bounce period. In addition, Eq. (37) gives the value of the betatron field required to drift the beam near the minor axis. Finally, the electron gyroradius around the guiding center can be minimized using Eqs. (28) and (29).

For the parameters of Table I, the value of the betatron field required if the equilibrium position of the beam is to be on the minor axis of the torus can be computed from Eq. (37) and is approximately 48 G. Similarly, when the vertical field is 35 G, the equilibrium position X_{eq} is located about 10.5 cm from the minor axis of the torus (see Fig. 5a). Therefore, by increasing the betatron field as

shown in Fig. 4, from 35 G to 48 G over a time period that is comparable to the beam bounce period, the beam equilibrium position will move from $X_{eq} = 10.5$ cm to $X_{eq} = 0$. Figure 5b shows the orbit of the reference electron for $B_{z0} = 48$ G, for 35 G, and for the combined field plotted in Fig. 4. This field consists of a 48-G time-independent field and a time-dependent "trapping" field that varies as

$$B_{tr} = \begin{cases} B_{tro} e^{-(t-t_0)/\tau}, & \text{for } t \geq t_0, \\ B_{tro}, & \text{for } t_0 \leq t, \end{cases}$$

where t_0 is the trapping initiation time. For the results of Fig. 5, the values of the various parameters of the "trapping" field are listed in Table III.

Over the first 20 ns, i.e., over a revolution around the major axis, the beam drifts 8 cm away from the injector, which is more than sufficient. However, the electron drifts around the new equilibrium position at $X_{eq} = Z_{eq} = 0$ very slowly. The total time required to complete the bounce in Fig. 5 is in excess of 1.3 μs.

To determine the sensitivity of the orbit to the initial azimuthal position of the injector, we made a series of runs with the injector always at the same X and Z but at different S positions. Figure 6 shows the results when the injector is moved from $S = L/4$ to $S = 0$. The remaining parameters for this run are identical to those of Fig. 5. It should be noticed that the final guiding-center radius, i.e., when the electron gyrates around $X = Z = 0$, is appreciably smaller in Fig. 6 than in Fig. 5. There is an additional difference between the results of these two runs, which is not apparent in the figures. In Fig. 6, at the injection point, the torsatron field is directed downwards, and thus the force $-ev_\theta B_z^t$ is directed radially outward. As a result, the initial motion of the electron is outward. In contrast, the $-ev_\theta B_z^t$ force at the injection point in Fig. 5 is radially inward and so is the initial motion of the electron.

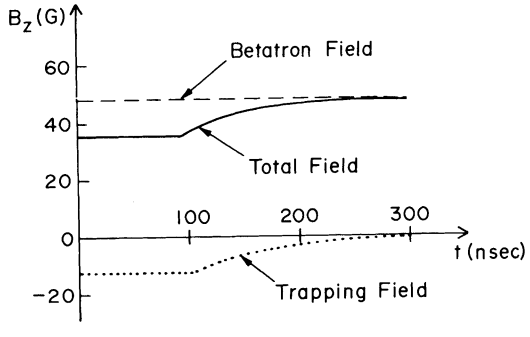

$$B_{tr} = \begin{cases} B_{tro}\, e^{-(t-t_0)/\tau}, & \text{for } t \geq t_0 \\ B_{tro}, & \text{for } t \leq t_0 \end{cases}$$

FIGURE 4 Betatron, trapping, and total vertical fields as functions of time.

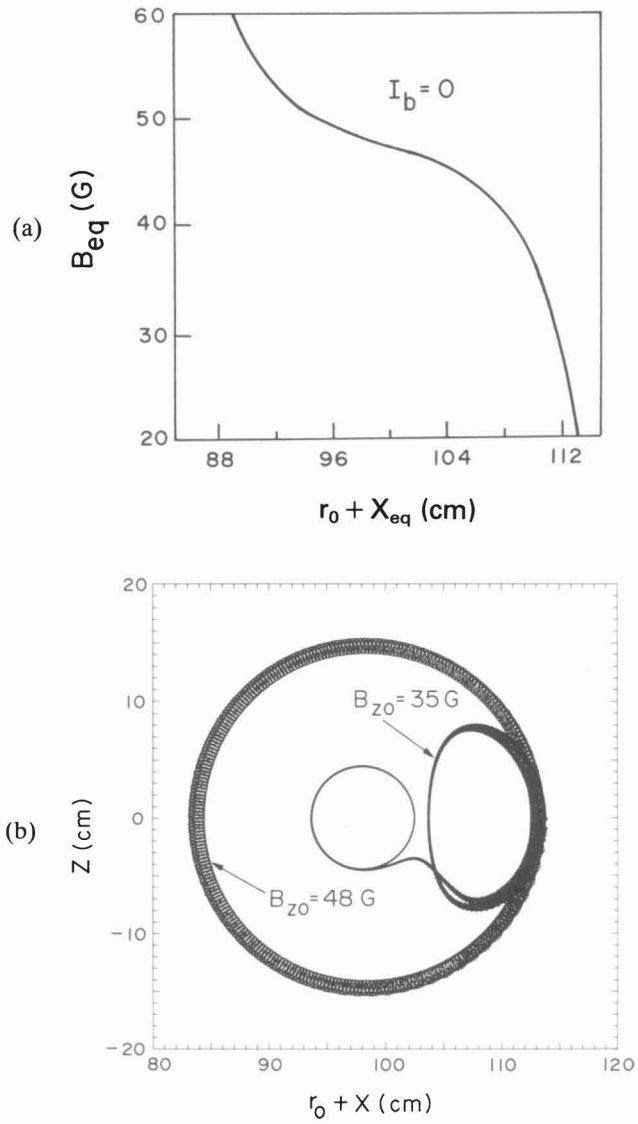

FIGURE 5 (a) Vertical magnetic field required to confine the beam at its equilibrium position, referred to the minor axis, for $I_b = 0$. (b) Orbit of reference electron at the beam centroid, injected at 114 cm from the major axis when $B_{z0} = 35$ G = constant and $B_{z0} = 48$ G = constant, and in the presence of the trapping magnetic field. The various parameters for this run are listed in Table III.

The results shown in Figs. 5 and 6 were obtained for zero electron beam current. However, the trapping mechanism remains applicable even at high beam current I_b. Results are shown in Fig. 7 for $I_b = 5.15$ kA. As shown in Fig. 7a, by increasing the magnetic field from 47 G to 57 GF, the equilibrium position moved from 104 cm to 100 cm. The rest of the parameters for this run are listed in Table

TABLE III

Parameters of The Runs Shown in Figs. 5 and 6

		Fig. 5	Fig. 6
Torus major radius, r_0 (cm)		100	100
Winding minor radius, ρ_0 (cm)		18	18
Toroidal chamber minor radius, a (cm)		20	20
$\alpha = 2\pi/L$ (cm^{-1})		0.1	0.1
Field strength factor, ε_t		−0.04275	−0.04275
Winding current, I (kA)		25	25
ℓ		2	2
Torsatron toroidal field, B_s (kG)		1.0	1.0
e-fold time, τ (ns)		100	100
Trapping initiated at time (ns)		100	100
Trapping field amplitude, B_{tr} (G)		−13	−13
Additional toroidal field, B_s^{ex} (kG)		3.0	3.0
Betatron field, B_{z0} (G)		48	48
External field index, n		0.5	0.5
Electron beam current, I_b (kA)		0	0
Initial $\gamma = \gamma_D$ (diode)		2.96	2.96
Initial positions (cm)	$X(t=0)$	14	14
	$Z(t=0)$	0	0
	$S(t=0)$	15.7	0
Initial velocities	$\dot{X}(t=0)$	0	0
	$\dot{Z}(t=0)$	0	0
	v_θ	0.941c	0.941c

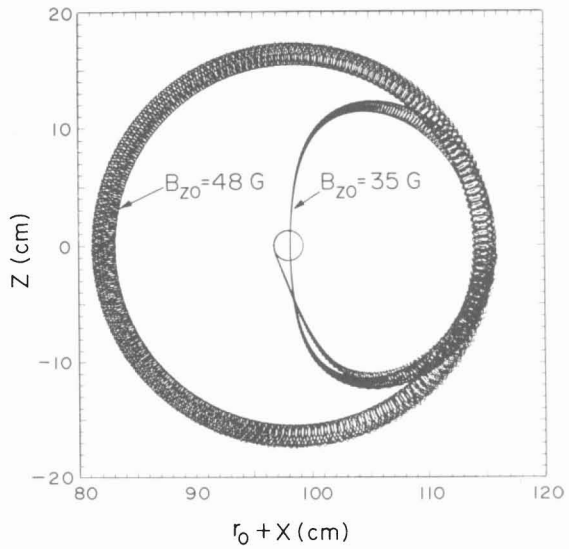

FIGURE 6 Same as Fig. 5, but with the injector at a new initial toroidal position ($S = 0$). The various parameters for this run are listed in Table III.

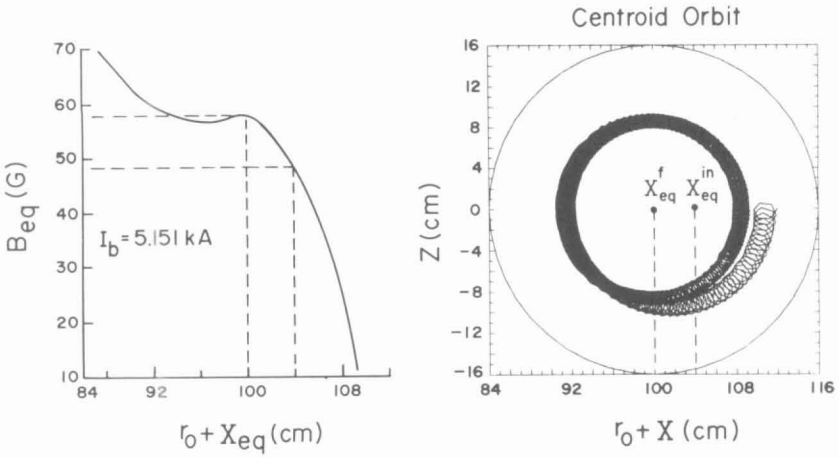

FIGURE 7 (a) Vertical magnetic field required to confine the beam at its equilibrium position, referred to the minor axis, for the parameters listed in Table IV. (b) Orbit of the reference electron located at the beam centroid, in the presence of the trapping field. The equilibrium position moves from 104 cm to 100 cm when the vertical field is increased from 47 G to 57 G. Initially, the beam is injected with its centroid located at 112 cm. Since the orbit of the fast motion of the particle has a 2 cm diameter, the average position of the particle (guiding center) and the injection position are different by about 1 cm.

TABLE IV

Parameters of The Run Shown in Fig. 7

Torus major radius, r_0 (cm)		100
Winding minor radius, ρ_0 (cm)		18
Toroidal chamber minor radius, a (cm)		16
$\alpha = 2\pi/L$ (cm^{-1})		0.06
Field strength factor, ε_t		−0.169776
Winding current, I (kA)		55
ℓ		2
Torsatron toroidal field, B_s (kG)		1.32
e-fold time, τ (ns)		200
Trapping initiated at time (ns)		0
Trapping field amplitude, B_{tr} (G)		−10
Additional toroidal field, B_s^{ex} (kG)		5.0
Betatron field, B_{z0} (G)		57
External field index, n		0.5
Electron beam current, I_b (kA)		5.151
Initial γ (at injection)		1.95
Diode gamma, γ_D		2.96
Minor beam radius, r_b (cm)		1.0
ν/γ		0.18
Initial positions (cm)	$X(t=0)$	12
	$Z(t=0)$	0
	$S(t=0)$	26.18
Initial velocities	$\dot{X}(t=0)$	0
	$\dot{Z}(t=0)$	0
	v_θ	0.858c

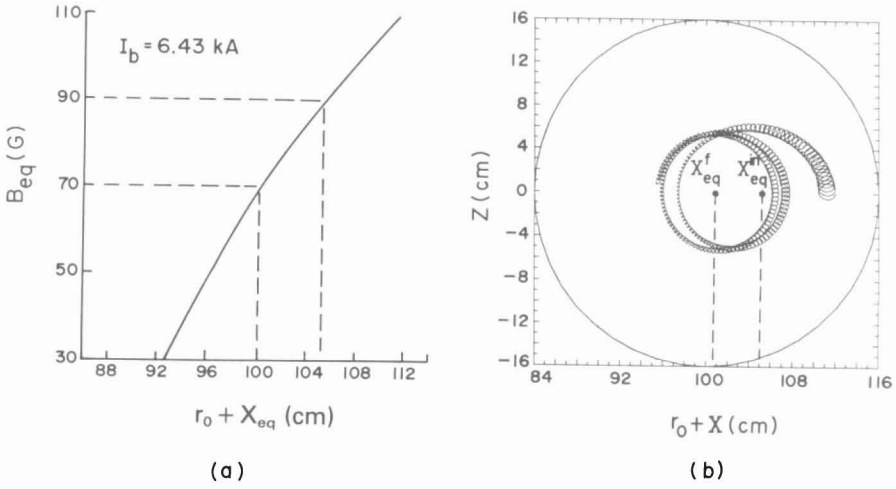

FIGURE 8 (a) Vertical magnetic field required to confine the beam at its equilibrium position, referred to the minor axis, for the parameters listed in Table V. (b) Orbit of the reference electron located at the beam centroid in the presence of the trapping field, when the rational transform induced by the self-fields overwhelms the transform of the external fields. In this case, the equilibrium position moves toward the minor axis by decreasing the vertical field.

IV. In this run, a swell as in the run shown in Fig. 8, the self-fields have been modeled to include the nonlinear cylindrical term, i.e., a^2 in Eqs. (33a) through (33d) has been replaced by $a^2(1-R^2/a^2)$. In addition, the quadratic vector potential that describes the betatron field has been replaced by the nonlinear vector potential

$$A_\theta^{\text{bet}} = B_{z0}\left[\left(\frac{r_0}{r_0+X}\right)^n \frac{(r_0+X)}{(2-n)} + \frac{r_0^2}{(r_0+X)}\frac{(1-n)}{(2-n)} + \frac{nZ^2}{2(r_0+X)}\right].$$

Finally the toroidal corrections to the torsatron field have been omitted.

At even higher beam current, the rotational transform induced by the self-fields overwhelms the vacuum transform, and the beam centroid rotates in the direction opposite that of the low-current case. Results are shown in Fig. 8. It should be noticed that the slope of the curve in Fig. 8a that describes B_{eq} vs X_{eq} is different from that in the low-current case. The results of Fig. 8 were obtained from the numerical integration of the exact equations of motion for a beam current of 6.43 kA. The remaining parameters for the run are listed in Table V.

When the small term P_θ/mcr_0 is neglected, the linearized constant of the motion [Eq. (47)] can be written

$$K_0 = q_1\left(\frac{X}{r_0}\right)^2 + q_2\left(\frac{Z}{r_0}\right)^2 - \frac{2\delta P_\theta}{mr_0^2\Omega_{z0}}\left(\frac{X}{r_0}\right), \tag{49}$$

where

$$q_1 = 1 - n - n_s r_b^2/a^2 + n_t,$$
$$q_2 = n - n_s r_b^2/a^2 + n_t.$$

TABLE V

Parameters of The Run Shown in Fig. 8

Torus major radius, r_0 (cm)		100
Winding minor radius, ρ_0 (cm)		18
Toroidal chamber minor radius, a (cm)		16
$\alpha = 2\pi/L$ (cm^{-1})		0.06
Field strength factor, ε_t		−0.102894
Winding current, I (kA)		20
ℓ		2
Torsatron toroidal field, B_s (kG)		0.48
e-fold time, τ (ns)		200
Trapping initiated at time (ns)		0
Trapping field amplitude, B_{tr} (G)		20
Additional toroidal field, B_s^{ex} (kG)		3.0
Betatron field, B_{z0} (G)		70
External field index, n		0.5
Electron beam current, I_b (kA)		6.43
Initial γ (at injection)		1.68
Diode gamma, γ_D		2.96
Minor beam radius, r_b (cm)		1.0
v/γ		0.28
Initial positions (cm)	$X(t=0)$	12
	$Z(t=0)$	0
	$S(t=0)$	26.18
Initial velocities	$\dot{X}(t=0)$	0
	$\dot{Z}(t=0)$	0
	v_θ	0.646c

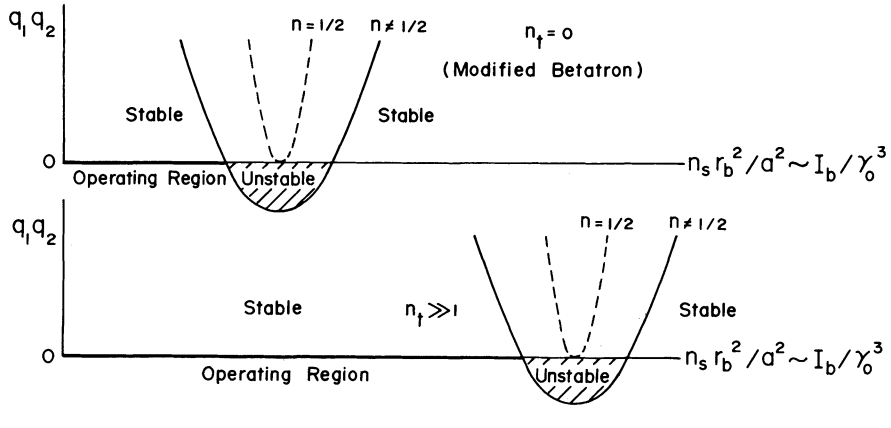

FIGURE 9 Plot of the product $q_1 \cdot q_2$ vs $n_s r_b^2/a^2$ for $n_t = 0$ (modified betatron) and $n_t \gg 0$ (modified betatron with strong focusing). The orbits are closed (stable) when $q_1 \cdot q_2 > 0$.

In these last expressions,

$$n_t = \frac{(\Omega_s^{ex}\varepsilon_t)^2 r_0 \alpha}{2\Omega_{z0}\,|\hat{\Omega}_{\theta 0})|}$$

is the torsatron field index, $\hat{\Omega}_{\theta 0} < 0$ is the combined toroidal field at r_0, and $n_s \equiv \omega_b^2/(2\gamma_0\Omega_{z0}^2)$ is the self-field index. According to Eq. (49), the macroscopic beam orbits are stable, provided $q_1 \cdot q_2 > 0$. Figure 9 shows the product $q_1 \cdot q_2$ as a function of $n_s r_b^2/a^2$ for $n_t = 0$ (modified betatron) and $n_t \neq 0$, i.e., a modified betatron with torsatron windings. Since $n_s r_b^2/a^2 \cong I_b/\gamma_0^3$, the parameter $n_s r_b^2/a^2$ decreases rapidly during acceleration. Therefore, in order to avoid crossing the instability gap when γ_0 increases, it is necessary to select the beam parameters in such a way that $n_s r_b^2/a^2$ is located in the left stable region during injection. However, in Fig. 8, $n_s r_b^2/a^2$ is located in the right stable region; therefore, it is likely that the beam will be lost during acceleration.

4. CONCLUSIONS

For $\omega_w < (\Omega_\theta/\gamma)$, we have derived two equations that describe the nonlinear transverse motion of the guiding center of the reference electron that is located at the beam centroid. Using these equations, we have obtained nonlinear expressions that predict very accurately the beam equilibrium position, even when $2\alpha R > 1$. Furthermore, by integrating analytically the guiding-center equations, we have obtained a constant of the motion that predicts approximately the guiding-center orbits in the transverse plane.

With the insight provided by these analytical results, we were able to develop a realistic trapping scheme that does not require the presence of a resistive wall and therefore is compatible with the relative slow acceleration of the modified betatron.

The proposed trapping scheme opens the possibility of adding strong focusing in a modified betatron accelerator. Such focusing may have several beneficial effects on the device, because (i) it will alleviate the difficulty associated with the orbit displacement resulting from the energy mismatch, (ii) it could alleviate the beam displacement associated with the diffusion of the self-magnetic-field, and (iii) it will improve the current-carrying capabilities of the device without requiring injection at higher energies.

REFERENCES

1. P. Sprangle and C. A. Kapetanakos, *J. Appl. Phys.* **119,** 1 (1978).
2. C. A. Kapetanakos, P. Sprangle, D. P. Chernin, S. J. Marsh, and I. Haber, *Phys. Fluids* **26,** 1634 (1983).
3. D. Chernin and P. Sprangle, *Particle Accelerators,* **12,** 85 (1982).
4. W. Manheimer and J. Finn, *Particle Accelerators* **14,** 29 (1983).
5. C. Agritellis, S. J. Marsh, and C. A. Kapetanakos, *Particle Accelerators* **16,** 155 (1985).
6. C. A. Kapetanakos and S. J. Marsh, *Phys. Fluids* **28,** 2263 (1985).

7. J. M. Grossman, T. M. Finn, and W. Manheimer, *Phys. Fluids* **29,** 695 (1985).
8. J. M. Grossman and W. M. Manheimer, *Particle Accelerators* **16,** 185 (1985).
9. W. M. Manheimer, *Particle Accelerators* **13,** 209 (1983).
10. D. Chernin and P. Sprangel, *Particle Accelerators* **12,** 101 (1982).
11. P. Sprangle and C. A. Kapetanakos, *Particle Accelerators* **14,** 15 (1983).
12. P. Sprangle and D. Chernin, *Particle Accelerators* **35,** 15 (1984).
13. C. A. Kapetanakos, P. Sprangle, and S. J. Marsh, *Phys. Rev. Lett* **49,** 741 (1982).
14. F. Mako, W. Manheimer, D. Chernin, F. Sandal, and C. A. Kapetanakos, *Phys. Fluids* **27,** 2211 (1984).
15. B. Hui and T. T. Lau, *Phys. Rev. Lett.* **53,** 2024 (1984).
16. N. Rostoker, *Comments Plasma Phys.* **6,** 91 (1980).
17. G. Barok and N. Rostoker, *Phys. Fluids* **26,** 856 (1983).
18. R. C. Davidson and H. S. Uhm, *Phys. Fluids* **25,** 2089 (1982).
19. H. S. Uhm and R. C. Davidson, *Phys. Fluids* **25,** 2334 (1982).
20. H. S. Uhm, R. C. Davidson, and J. Petilo, *Phys. Fluids* **28,** 2537 (1985).
21. H. Ishizuka, G. Lindley, B. Mandelbaum, A. Fisher, and N. Rostoker, *Phys. Rev. Lett.* **53,** 266 (1984).
22. J. Golden, J. Pasour, D. E. Pershing, K. Smith, F. Mako, S. Slinker, F. Mora, N. Orick, R. Altes, A. Fliflet, P. Champney, and C. A. Kapetanakos, *IEEE Trans. Nucl. Sci.* **NS-30,** 2114 (1983).
23. C. W. Roberson, A. Mondelli, and D. Chernin, *Phys. Rev. Lett.* **50,** 507 (1983).
24. C. A. Kapetanakos, P. Sprangle, S. J. Marsh, D. Dialetis, C. Agritellis, and A. Prakash, *Particle Accelerators,* to be published.
25. P. Sprangle and C. A. Kapetanakos, *Particle Accelerators* **18,** 203 (1986).
26. T. G. Northrop, *The Adiabatic Motion of Charged Particles* (Interscience, New York, 1963).